Research Square

Preprints are preliminary reports that have not undergone peer review.
They should not be considered conclusive, used to inform clinical practice,
or referenced by the media as validated information.

Multi-scenario ecosystem service trade-offs and ecological security patterns in the upper Yongding River Basin, China (1990-2024)

Yan Jiang

jiangyan@iwhr.com

China Institute of Water Resources and Hydropower Research

Gang Wang

Tianjin University

Xiaoyan Zhang

Hebei Agricultural University

Jingfeng Hu

China University of Geosciences (Beijing)

Research Article

Keywords: Ecosystem services, Trade-offs, Ordered Weighted Averaging, Ecological security pattern, MSPA, Circuit theory

Posted Date: November 13th, 2026

DOI: https://doi.org/10.21203/rs.3.rs-11592346/v1

License: This work is licensed under a Creative Commons Attribution 4.0 International License.
Read Full License

Additional Declarations: No competing interests reported.

Multi-scenario ecosystem service trade-offs and ecological security patterns in the upper Yongding River Basin, China (1990-2024)

Yan Jiang[a,*]

Gang Wang[b,c]

Xiaoyan Zhang[c]

Jingfeng Hu[d]

a China Institute of Water Resources and Hydropower Research, Beijing, China

b Tianjin University, Tianjin, China

c Hebei Agricultural University, Hebei, China

d China University of Geosciences (Beijing), Beijing, China

Corresponding author. E-mail: jiangyan@iwhr.com

Tel.: 86 13611063827

ORCID: Yan Jiang: 0009-0003-6224-6583; Gang Wang: 0009-0005-6444-0149; Xiaoyan Zhang: 0009-0007-0642-8955; Jingfeng Hu: 0009-0002-6642-3519.

Acknowledgements

This work was supported by the National Science and Technology Major Project of China (grant number 2025ZD1202102) and the Key Research and Development Program of Hebei Province (grant number 22376201D).

Highlights

- Seven-scenario OWA analysis links ecosystem-service trade-offs with ecological security patterns.
- A moderate weighting scenario (S5, $\alpha = 2$) is the preferred scenario under the tested metric.
- Habitat fragmentation coexists with more connected and redundant corridor network.
- Ecological sources have consolidated into fewer patches from 1990 to 2024, but the largest primary source has shrunk substantially.
- The framework supports conservation zoning and adaptive basin management in the region.

Abstract

Context. Balancing multiple ecosystem services (ESs) is a prerequisite for constructing a stable ecological security pattern (ESP); however, conventional ESP studies rarely account for service trade-offs when selecting conservation priorities. Therefore, explicitly linking these trade-offs to ESP dynamics is essential for evidence-based landscape conservation planning.

Objectives. This study used the upper Yongding River Basin (44,006 km²), a key water source and ecological barrier for the Beijing-Tianjin-Hebei region, as the study area. We aimed to combine seven OWA weighting scenarios with ESP construction and evaluate the resulting network from 1990 to 2024.

Methods. Six ESs were quantified using InVEST for 1990, 2000, 2010, and 2024. The OWA operator generated seven trade-off scenarios (weighting parameters 0.001–1000), and the preferred scenario under the tested metric was used with MSPA, Circuitscape and four graph-theoretic indices (α, β, γ, ρ) to construct and assess the ESP.

Results. Scenario S5 (α = 2) achieved the highest average conservation efficiency in every period. The MSPA core share declined from 56.10% to 48.26%, while the bridge share increased to 40.86%. Ecological sources contracted from 23 patches (9,190.8 km²) in 1990 to 14 patches (5,852.4 km²) in 2024. The network became more compact and topologically redundant, even as habitats fragmented and sources consolidated. Protecting remaining primary sources and restoring bridge-class corridors could therefore improve connectivity at lower conservation cost.

Conclusions. The workflow provides a basin-specific basis for balancing service trade-offs and supports conservation zoning and adaptive basin management. S5 is a local preference under the tested inputs and not a general rule.

Keywords: Ecosystem services; Trade-offs; Ordered Weighted Averaging; Ecological security pattern; MSPA; Circuit theory

1. Introduction

Ecosystem services (ESs) are the benefits that people obtain from ecosystems, and underpin human well-being and regional sustainable development (Daily 1997; Costanza et al. 1997; Millennium Ecosystem Assessment 2005). Because ecosystem structure, function and human preferences vary in space, ESs interact through trade-offs and synergies rather than changing independently (Bennett et al. 2009; Raudsepp-Hearne et al. 2010). Understanding and managing these interactions is central to ecology, geography and conservation planning (Seppelt et al. 2011; Braat and de Groot 2012; Wu 2013).

The ecological security pattern (ESP) is a spatial configuration of ecological sources, corridors and strategic nodes. It safeguards key ecological processes and links ES assessment with landscape-scale conservation practice (Yu 1996; Peng et al. 2018). ESP construction draws on mapped and modeled ES supply and demand (Burkhard et al. 2012; Crossman et al. 2013). In the prevailing paradigm, ecological sources are identified from areas of high ES supply or habitat importance. Corridors are simulated using least-cost-path or circuit-theory methods (Adriaensen et al. 2003; McRae et al. 2008). Recent applications combine multi-criteria decision making with circuit theory (Yu et al. 2022), MSPA with least-cost-path modeling (Li et al. 2024), or MSPA with circuit theory (Zhai and Huang 2022). Two limitations persist. First, source identification often uses a single service or averages normalized services with equal weights, which implicitly assumes that all ESs vary together. Services such as water yield, soil retention, carbon storage and habitat quality frequently conflict (Bennett et al. 2009); therefore, identified priorities can depend strongly on the chosen weights. Second, most ESP studies are static and represent a single year. Few studies track changes in sources, corridors and network topology over decades (Zhang et al. 2025). Few connect these patterns to future land-use scenarios (Li et al. 2023; Wu et al. 2025). Such changes are essential for adaptive management.

The Ordered Weighted Averaging (OWA) operator addresses the first limitation. It assigns order weights to ranked criterion values and tunes a weighting parameter. This generates a continuous family of rules from risk-averse minimum-type aggregation to risk-taking maximum-type aggregation (Yager 1988, 1996). OWA allows alternative conservation priorities to be compared under explicit trade-off scenarios. It has been used to construct ecological security patterns that reconcile ecosystem-service trade-offs (Guo et al. 2022; Liu et al. 2023; Yin et al. 2022). Morphological spatial pattern analysis (MSPA) classifies the foreground of a binary map into seven mutually exclusive classes (core, islet, perforation, edge, bridge, loop and branch). This provides a geometry-sensitive basis for identifying structurally important habitats (Vogt et al. 2007; Soille and Vogt 2009). Circuit-theory corridor modeling (McRae et al. 2008) completes this chain with graph-theoretic network indices (Kansky 1963; Haggett and Chorley 1969; Forman and Godron 1986; Cook 2002). The combined methods link scenario trade-off analysis, pattern construction and topology evaluation. In this study, multi-scenario refers specifically to seven OWA weighting scenarios, not to future land-use or climate projections. The main contribution over prior OWA, MSPA and Circuitscape studies is the four-period dynamic assessment, explicit comparison of weighting scenarios, and systematic resistance-surface sensitivity testing. The α values are mathematical weighting parameters, and the terms risk-taking and risk-averse describe aggregation rules rather than empirically elicited stakeholder risk attitudes. The resulting zones are a technical screening framework for subsequent socioeconomic evaluation. However, the node-edge abstraction used in network analysis often ignores patch stability and internal heterogeneity (Jiang et al. 2024).

The upper Yongding River Basin is upstream of the Guanting Reservoir and supplies water to Beijing. It occupies a semi-arid mountain-basin transition zone in northern China. It has experienced substantial land-use changes and ecological restoration over the past three decades (Yang and Huang 2026; Ouyang et al. 2016). An ESP for this basin is directly relevant to the ecological security of the Beijing-Tianjin-Hebei region. We addressed four objectives. First, we quantified six ESs (water yield, soil retention, carbon storage, habitat quality, and total nitrogen and phosphorus export control) for 1990, 2000, 2010 and 2024. Second, we constructed seven OWA scenarios and selected the preferred scenario under the tested metric for ecological priority zones based on conservation efficiency. Third, we constructed the ESP by coupling MSPA-based source identification with Circuitscape-based corridor modeling. Fourth, we analyzed changes in the pattern and its network topology from 1990 to 2024. The results provide a reproducible workflow for this basin. S5 is interpreted as a basin-specific preference under the selected inputs; application to other basins requires independent validation.

In plain terms, this study mapped six ecosystem services, compared seven ways of weighting their trade-offs, selected the weighting that was preferred under the tested metric in this basin, identified ecological sources and corridor networks, and tracked how those networks changed over four periods.

2. Materials and methods

Study area

The upper Yongding River Basin (approximately 112° to 117° E, 39° to 41° N) lies in the transition belt among the Inner Mongolia Plateau, Shanxi Plateau, and North China Plain. It covers parts of Shanxi, Hebei and Inner Mongolia and adjoins Beijing to the east (Fig. 1). The basin covers an area of approximately 44,006.2 km², with an elevation ranging from 64 to 2,817 m and terrain sloping from northwest to southeast. It has a temperate continental monsoon climate, with precipitation concentrated in summer and runoff and water yield concentrated along the river valleys. It is the principal recharge area of the Guanting Reservoir and a sand-source control belt upwind of the capital. The basin contributes to water conservation, soil retention and habitat maintenance. Intensive agriculture, mining and urban expansion have placed considerable pressure on its ecosystems. This makes the basin a useful site for examining ES trade-offs and ecological security.

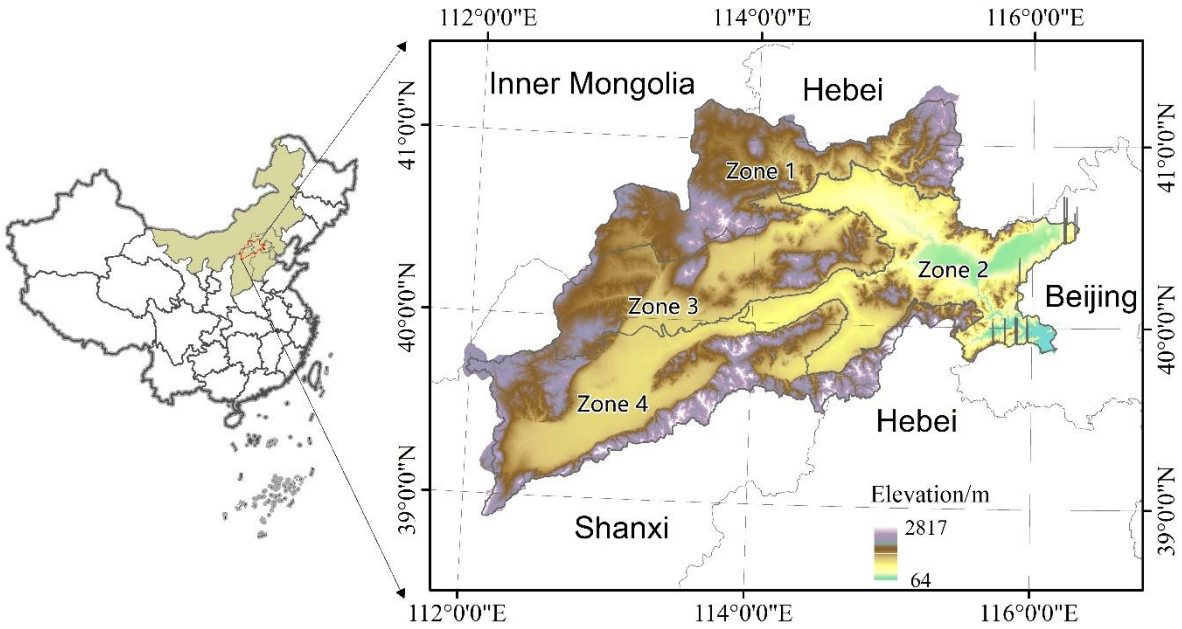


Fig. 1. Location of the upper Yongding River Basin.

Data sources and preprocessing

Multi-source datasets from 1990, 2000, 2010 and 2024 were assembled and resampled to a common 30 m grid in a shared projected coordinate system. The inputs included (i) land-use/land-cover data from the 30 m annual China Land Cover Dataset (Yang and Huang 2026); (ii) a digital elevation model (DEM) and derived slope; (iii) interpolated meteorological observations of precipitation, temperature, and potential evapotranspiration from national stations; (iv) soil texture, depth, and organic matter from the Harmonized World Soil Database and regional soil surveys; (v) NDVI and net primary productivity (NPP) products; and (vi) watershed and administrative boundaries, river networks, and road networks. All raster layers were clipped to the basin boundary. Vector layers were used to obtain source patch and corridor statistics.

For cross-year comparability, the four CLCD grids were clipped and aligned to a common 30 m reference grid. Background values were excluded, and the 2024 grid, which had a small origin shift, was aligned by nearest-neighbor resampling. Between 1990 and 2024, cropland decreased from 21,724.1 to 17,816.4 km², forest increased from 4,186.4 to 6,733.3 km², grassland decreased from 16,776.1 to 16,413.7 km², and wetland increased from 1,075.5 to 2,787.9 km². The land-use transition analysis showed that 27.26% of valid pixels changed during this period.

Analytical framework

The analytical framework comprises four linked steps (Fig. 2). First, multi-source data were prepared and six ESs were quantified using the InVEST model for the four study periods. Second, the six normalized ES layers were aggregated using the OWA operator to generate seven trade-off scenarios by varying the weighting parameter α. Conservation efficiency was then calculated, and the scenario with the highest average efficiency was selected to delineate ecological priority zones. Third, the priority zones were processed with MSPA. Core patches above a size threshold were extracted as network nodes and graded, MSPA classes were reclassified into a resistance surface, and ecological corridors were identified using Circuitscape. Fourth, changes in sources and corridors from

1990 to 2024 were analyzed, and the topology of the ecological network was evaluated using four graph-theoretic indices.

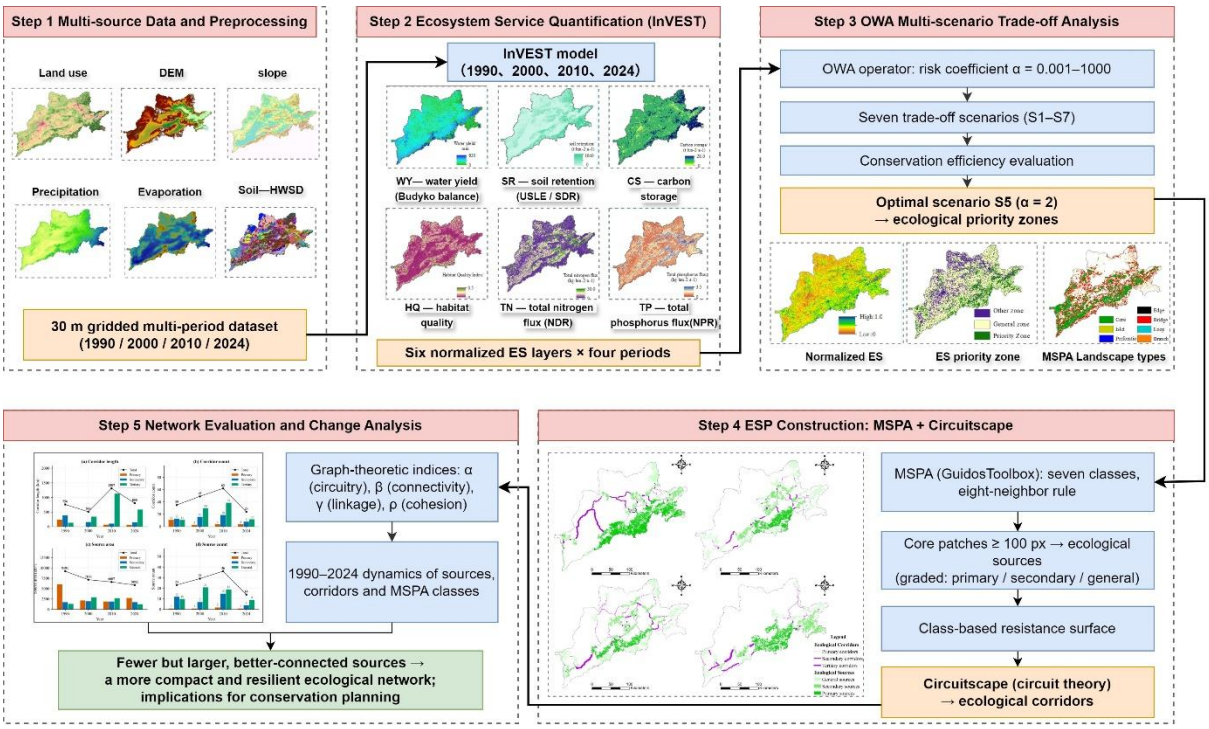


Fig. 2. Technical framework for constructing the ecological security pattern from OWA-based multi-scenario ecosystem-service trade-offs (WY: water yield; SR: soil retention; CS: carbon storage; HQ: habitat quality; TN: nitrogen export control; TP: phosphorus export control).

Quantification of ecosystem services

Six ESs were quantified for each period using the corresponding InVEST modules (Sharp et al. 2020); the formulas and variable definitions are summarized in Table 1. Water yield was estimated using the water yield module based on the Budyko water-energy balance (Donohue et al. 2012), in which the annual yield was precipitation minus actual evapotranspiration. Soil retention was calculated using the sediment delivery ratio module as potential erosion (RKLS) minus actual erosion (USLE) from the universal soil loss equation (Wischmeier and Smith 1978). Carbon storage was quantified using the InVEST Carbon Storage and Sequestration module using the total current carbon-storage raster tot_c_cur_[suffix].tif. This raster sums the aboveground, belowground, soil and dead-matter carbon pools mapped to each land-use type; the dead-matter pool was set to zero for all land-use types. The raster is reported in metric tons per hectare. Habitat quality was modeled from land-use-based threat sources, decay distances and habitat sensitivity scores using a half-saturation degradation function. Total nitrogen and phosphorus exports were estimated using the nutrient delivery ratio (NDR) module. This module routes the nutrient load of each pixel to streams according to hydrological connectivity and retention efficiency. All service layers were min-max normalized to [0, 1] using a single minimum and maximum calculated across all four periods before aggregation. Complete parameter values, biophysical tables, software versions and validation data should be reported in a supplementary file. The complete InVEST parameter tables are provided in Online Resources S1–S6. InVEST version 3.19.0 was used for all service calculations. The pixel-level raster outputs n_total_export.tif and p_surface_export.tif were used for TN and TP, respectively. Both rasters are reported in $kg \cdot ha^{-1} \cdot year^{-1}$ and represent the nutrient reaching streams, not the nutrient retained on the landscape. Before min-max normalization

and OWA aggregation, the TN and TP export values were inverted so that lower export indicated higher performance. The service layers should therefore be interpreted as model-based screening maps rather than independently validated service estimates. Percentages are reported to two decimal places, areas to one decimal place, and network indices to three decimal places.

Table 1. Calculation methods for the six ecosystem services (InVEST model).

Ecosystem service	Formula	Description
Water yield (WY)	$Y_{xj} = \left(1 - \frac{AET_{xj}}{P_x}\right) \times P_x$	Y_{xj} is the annual water yield of grid x under land-use type j; AET_{xj} is the average annual evapotranspiration; and P_x is the average annual precipitation.
Soil retention (SR)	$SC = RKLS - USLE = R \times K \times LS - R \times K \times LS \times C \times P$	SC is soil retention; R is the rainfall erosivity factor; K is the soil erodibility factor; L and S are the slope-length and slope factors; C is the vegetation cover and management factor; P is the support-practice factor.
Carbon storage (CS)	$C_{xj} = C_{soil} + C_{abovej} + C_{belowj}$	C_{xj} is the carbon storage of grid x under land-use type j; C_{soil}, C_{abovej} and C_{belowj} are soil organic, aboveground and belowground carbon densities of type j (the dead-matter pool was set to zero for all land-use types; carbon storage is therefore the sum of soil, aboveground and belowground pools).
Habitat quality (HQ)	$Q_{xj} = H_j \left[1 - \left(\frac{D_{xj}^z}{D_{xj}^z + k^z}\right)\right]$	Q_{xj} is the habitat quality index of grid x in land-use type j; H_j is the habitat suitability of type j; D_{xj} is the habitat degradation degree of grid x in type j; k is the half-saturation constant; z is the default model parameter.
Nitrogen export control (TN)	$X_i^N = load_i^N \times NDR_i$	X_i^N is the nitrogen export of grid i; $load_i^N$ is the nitrogen load; NDR_i is the nutrient delivery ratio determined by hydrological connectivity and retention efficiency along the flow path.
Phosphorus export control (TP)	$X_i^P = load_i^P \times NDR_i$	X_i^P is the phosphorus export of grid i; $load_i^P$ is the phosphorus load; NDR_i is defined as above, with phosphorus-specific retention parameters.

OWA-based multi-scenario trade-off analysis

To represent different mathematical weighting preferences toward ES trade-offs, the six normalized services were aggregated at the pixel scale using the OWA operator (Yager 1988). For a given pixel, the six service values were ranked in descending order $v_1 \le v_2 \le \cdots \le v_6$, and the aggregated comprehensive ES value is

$$\mathrm{OWA} = \sum_{i=1}^{n} w_i \, v_i,$$

where $n = 6$ and w_i are the order weights associated with rank position i. Following the regular increasing monotone quantifier approach (Yager 1996), the weights are derived from a weighting parameter α as

$$w_i = \left(\frac{i}{n}\right)^{\alpha} - \left(\frac{i-1}{n}\right)^{\alpha}.$$

When $\alpha < 1$, the weight concentrates on the highest-ranked value (risk-taking, low trade-off); when $\alpha = 1$, all services are weighted equally (maximum trade-off); when $\alpha > 1$, the weight shifts toward the lowest-ranked values (risk-averse). Seven scenarios (S1 to S7) were designed with α = 0.001, 0.1, 0.5, 1, 2, 10 and 1000 (Table 2). The degree of trade-off embodied by each weight vector was measured by the normalized entropy-type dispersion

$$T = -\frac{1}{\ln n}\sum_{i=1}^{n} w_i \ln w_i,$$

which approaches 0 when a single rank dominates and 1 when the weights are uniform.

Conservation efficiency and scenario selection

The OWA analysis was implemented in MATLAB. The input rasters were six min-max normalized services. Pixels with a NoData value of -9999 were converted to NaN, and only pixels with valid values in all six services were used. For each pixel, the service values were sorted in descending order and multiplied by the order weights. The OWA score map was then classified using the 20th and 80th percentiles (q20 and q80). Scores above q80 were ecological priority areas, scores at or below q20 were non-ecological space, and the remaining pixels were general ecological space. Conservation efficiency was calculated from the original service values inside the priority area relative to the basin mean.

For each scenario, pixels above the threshold of the aggregated OWA value were delineated as candidate ecological priority zones. The conservation efficiency of scenario k for service j was defined as the ratio of the mean normalized value of service j inside the priority zone to that over the whole basin:

$$E_{k,j} = \frac{\bar{v}_j^{zone(k)}}{\bar{v}_j^{basin}}, \qquad \bar{E}_k = \frac{1}{6}\sum_{j=1}^{6} E_{k,j}.$$

A scenario with $\bar{E}_k > 1$ conserves services more efficiently than the basin average, following the logic of balancing multiple services when setting conservation priorities (Zhang et al., 2015). The scenario with the highest average efficiency across the four periods was selected as the preferred scenario under the tested metric, and its priority zones were used in the subsequent MSPA.

Five sensitivity analyses were performed using the OWA workflow. The weighting parameter α varied, each service was removed in turn, Monte Carlo noise was added, q20/q80 thresholds were changed, and Min-Max, Z-score, rank, and per-pixel normalizations were compared. The key results are summarized in the Online Resource S10.

MSPA and ecological source identification

Linkage Mapper 3.0.0 was run on ArcGIS Desktop 10.8 with an ArcInfo license. For each year, the core-node polygon shapefile core_nodes_year.shp used the gridcode field, and resistance.tif provided the resistance raster in the Krasovsky_1940_Albers projected coordinate system. Build Network and Map Linkages generated adjacency and least-cost links, respectively. Centrality Mapper used Circuitscape 4.0.7 in pairwise mode, with resistance.tif as the resistance raster and focal_nodes.tif as the focal-node raster. Linkage Priority ranked the corridors. The Circuitscape run logs reported one connected network component for each period.

The binary foreground obtained from the preferred-scenario priority zones was classified by the MSPA into seven mutually exclusive classes (core, islet, perforation, edge, bridge, loop and branch) (Vogt et al. 2007; Soille and Vogt 2009). The classification used an eight-neighbor rule and a fixed edge width in the GuidosToolbox. Core patches of at least 100 pixels were extracted as ecological sources, nodes of the network, and graded as primary, secondary or general using natural breaks in CF_Central, a current-flow centrality measure from Linkage Mapper and Circuitscape.

MSPA-based resistance surface and Circuitscape corridor identification

Rather than relying on subjectively weighted resistance factors, the resistance surface was derived directly from the MSPA classification. Each pixel was assigned the resistance of its MSPA class, on the assumption that structurally important classes are easier to traverse. Ordinal values were 1 for the core, 5 for the bridge, 8 for the loop, 15 for the branch, 20 for the edge, 30 for perforation, 80 for islet, and 100 for the background matrix. Ecological corridors were then identified using Circuitscape (McRae et al. 2008; Zhai and Huang 2022; Zhang et al. 2025), which treats the landscape as an electrical circuit. Core patches served as the source and sink nodes. The resulting cumulative current-density map delineated areas channeling ecological flows. Pixels with high current density were extracted as corridors and graded as primary, secondary or tertiary by thresholding current density according to their contribution to connectivity. To test this assumption, three alternative resistance surfaces were generated by compressing the non-core resistance gaps, expanding those gaps, and swapping the Bridge and Loop ranks. Each scheme was processed using the same Circuitscape and Linkage Mapper workflow. The resulting LCP-weighted cost-distance rasters, corridor grades, and source-pair connectivity were compared with the baseline. The key metrics are summarized in Online Resource S11.

Network topology indices

The ecological network was abstracted as an undirected planar graph $G = (V, L)$, with the node set V representing ecological source patches and the edge set L representing the corridors connecting them, following the conventional abstraction in which each corridor is an edge linking two sources. Four graph-theoretic indices (Kansky 1963; Haggett and Chorley 1969; Forman and Godron 1986; Cook 2002; Jiang et al. 2024) were computed for each period: α measures loops, β measures links per source, γ measures realized links relative to the planar maximum, and ρ is corridor density. The formulas are as follows:

$$\alpha = \frac{L - V + 1}{2V - 5},$$

$$\beta = \frac{L}{V},$$

$$\gamma = \frac{L}{3(V - 2)},$$

$$\rho = \frac{D}{A},$$

where the circuitry index α measures the degree of closed loops (network redundancy), the connectivity index β is the mean number of corridors per node, the cohesion index γ is the ratio of realized corridors to the planar-graph

maximum, and the corridor density ρ expresses the total corridor length D (km) per unit basin area (km²), giving corridor density in km/km² .

3. Results

Conservation efficiency is defined as the ratio of the mean service value within a priority zone to the basin-wide mean service value. A value exceeding 1 signifies a concentration of services above the average rather than independently assessed protection outcomes. Natural breaks refer to data-driven class boundaries used to categorize sources and corridors. CF_Central and Current_Flow_Centrality represent centrality scores derived from the Linkage Mapper and Circuitscape, respectively; higher scores denote more significant positions within the network. Connectivity is summarized by four network indices: α, which quantifies loops; β, which measures links per source; γ, which assesses realized links relative to the planar maximum; and ρ, which indicates corridor density.

Spatial pattern of ecosystem services

The six model-based ES screening maps varied considerably across the basin (Fig. 3). Water yield (0–630 mm) increased toward the eastern river valleys near Beijing, where precipitation and runoff converge. Soil retention (0 to 1,040 t·ha^{-1}·year^{-1}·hm^{-2} ·a^{-1}) was concentrated in steep, vegetated mountain belts, whereas broad intermountain basins retained little soil. Carbon storage (0 to 28 t/ha· hm^{-2}) The habitat quality index (0 to 0.5) was highest in the forested mountains along the northern and southwestern margins. Both services were lowest in the cultivated and built-up lowland areas. Total nitrogen and phosphorus export-control indicators (up to 30 and 3.5 kg/ha/year·hm^{-2}·a^{-1}, respectively) followed the river network. The largest exports occurred along the main channels and their riparian farmlands. Regulating and supporting services were concentrated in the mountains, whereas high water yields and nutrient export control indicators were concentrated in the valleys, matching the trade-offs examined below.

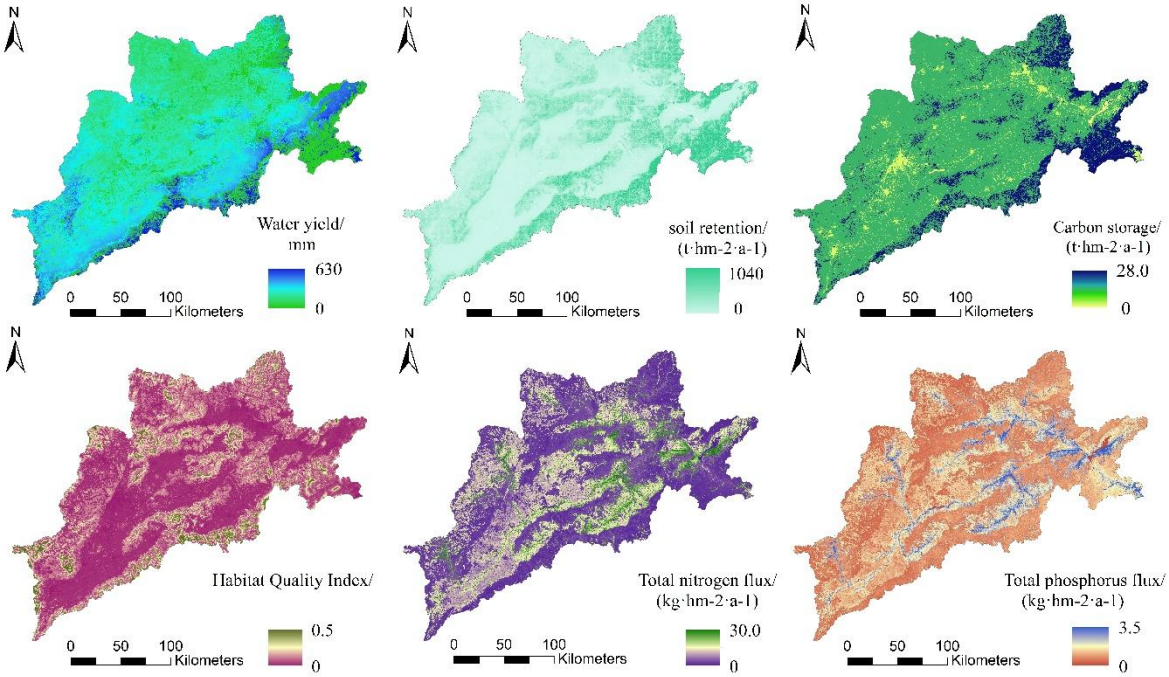


Fig. 3. Spatial distribution of ecosystem services in the Upper Yongding River Basin.

Weight combinations and trade-off degrees of the scenarios

The seven OWA scenarios spanned the full range of weighting scenarios (Table 2). Under S1 (α = 0.001), the highest rank carried a weight of 0.9982 and the trade-off degree was nearly zero (0.0021), representing maximum-type aggregation. As α increased, the weights were redistributed across ranks. The equal-weight scenario S4 (α = 1) had the maximum trade-off degree of 1. Under S5 (α = 2), the weights rose from 0.0278 to 0.3056 with a high but sub-maximal trade-off degree (0.7454). Under S6 (α = 10), the lowest rank reached a weight of 0.8385. Under S7 (α = 1000), only the lowest-ranked service was retained (trade-off degree 0).

Table 2. Weight combinations and trade-off degrees of the seven OWA scenarios.

Scenario	α	w_1	w_2	w_3	w_4	w_5	w_6	Trade-off
S1	0.001	0.9982	0.0007	0.0004	0.0003	0.0002	0.0002	0.0021
S2	0.1	0.8360	0.0600	0.0371	0.0272	0.0217	0.0181	0.1960
S3	0.5	0.4082	0.1691	0.1298	0.1094	0.0964	0.0871	0.7014
S4	1	0.1667	0.1667	0.1667	0.1667	0.1667	0.1667	1.0000
S5	2	0.0278	0.0833	0.1389	0.1944	0.2500	0.3056	0.7454
S6	10	0	0	0.0010	0.0164	0.1442	0.8385	0.1821
S7	1000	0	0	0	0	0	1	0

Conservation efficiency and scenario selection

Across the four periods (Table 3), S5 (α = 2) consistently obtained the highest average conservation efficiency. The values were 1.2944, 1.2649, 1.2389 and 1.2729 in 1990, 2000, 2010 and 2024. S5 exceeded both equal-weight S4 and more extreme scenarios. Therefore, it was selected as the preferred scenario under the tested metric because it maintained a high degree of trade-off among the six services while rewarding pixels where several services are simultaneously high. The complete service-specific conservation efficiencies are provided in Online Resource S8. Sensitivity analysis showed that α values from 0.1 to 1 produced priority areas with Spearman correlations of at

least 0.95, Kappa values of at least 0.89, and an overlap of at least 93%. The selected S5 (α = 2) had moderate overlap with the equal-weight baseline (61.9%) but remained the most efficient scenario. Varying the priority threshold between 15% and 30% preserved the core of the q20/q80 priority area. Ten percent input noise changed only 5.5% of class assignments. Removing A3 changed approximately 46% of the priority area, identifying A3 as the most influential service.

Table 3. Average conservation efficiency for each scenario from 1990 to 2024. The bold values indicate the preferred scenario under the tested metrics (S5).

Scenario	α	1990	2000	2010	2024
S1	0.001	1.0624	1.0752	1.0713	1.0838
S2	0.1	1.1828	1.1420	1.1331	1.1586
S3	0.5	1.2466	1.2171	1.2007	1.2142
S4	1	1.2638	1.2400	1.2181	1.2337
S5	**2**	**1.2944**	**1.2649**	**1.2389**	**1.2729**
S6	10	1.1804	1.0956	1.0589	1.1229
S7	1000	1.1542	1.0652	1.0346	1.0998

Changes in morphological spatial pattern

Fig. 4 shows the normalized comprehensive ES values, ecological priority zones of the preferred scenario and MSPA classes for the four periods; Table 4 summarizes the MSPA statistics. The core area, the backbone of the pattern, declined continuously from 12,295.0 km² (56.10%) in 1990 to 10,571.7 km² (48.26%) by 2024. This resulted in a net loss of 1,723.3 km². The bridge area grew steadily from 7,199.4 km² (32.85%) to 8,949.0 km² (40.86%) and became the second most dominant class. The islet area fluctuated from 1,501.0 to 1,488.9 km², with a dip to 1,209.0 km² in 2010. Perforation, edge, loop, and branch classes together accounted for less than 5% in all years, although edge and branch increased slightly. The Sankey diagram of class transitions (Fig. 5) shows that the dominant change pathway was the conversion of the core to the bridge. A substantial share of the 1990 core shifted successively into bridge and other connecting classes between 2000 and 2024. This included 10,647.2 km² of persistent core and reflects the erosion of large habitat blocks into elongated connectors.

Table 4. MSPA statistics of the foreground from 1990 to 2024. The areas are in km² and the percentages refer to the foreground.

Type	**Code**	**Area**	**%**	**Area**	**%**	**Area**	**%**	**Area**	**%**
		1990		2000		2010		2024	
Core	1	12 295.0	56.10	11 177.1	51.00	11 113.0	50.71	10 571.7	48.26
Islet	2	1 501.0	6.85	1 365.4	6.23	1 209.0	5.52	1 488.9	6.80
Perforation	3	7.8	0.04	11.6	0.05	12.6	0.06	12.1	0.06
Edge	4	12.0	0.05	14.2	0.06	15.0	0.07	14.7	0.07
Bridge	5	7 199.4	32.85	8 495.0	38.76	8 746.9	39.91	8 949.0	40.86
Loop	6	615.6	2.81	574.5	2.62	539.7	2.46	563.0	2.57
Branch	7	285.0	1.30	278.0	1.27	279.8	1.28	304.2	1.39

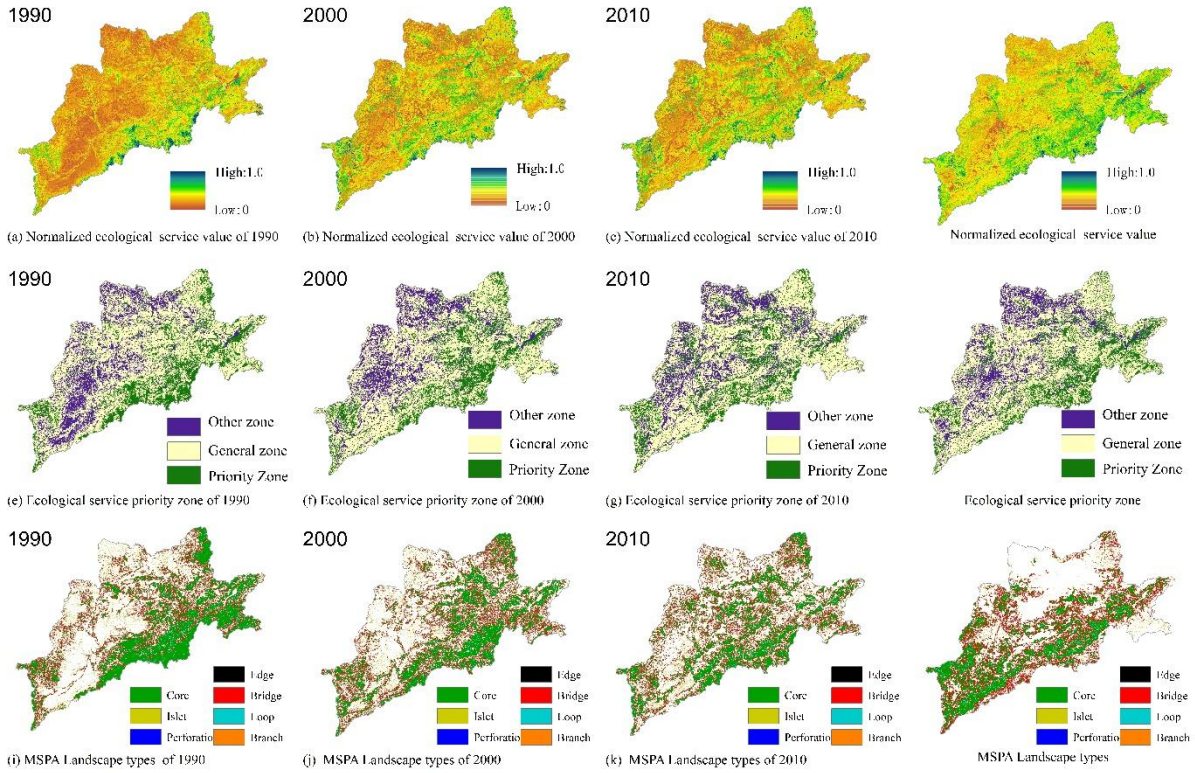


Fig. 4. Normalized comprehensive ecosystem service value (a-d), ecological priority zones (e-h), and MSPA landscape types (i-l) from 1990 to 2024.

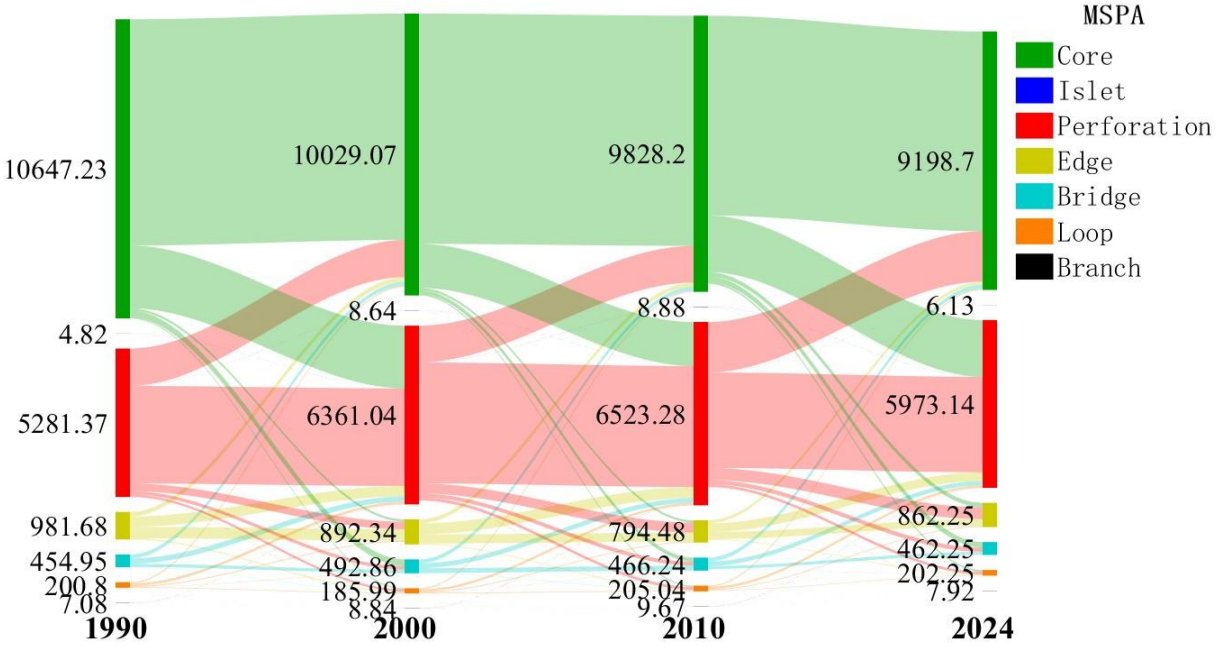


Fig. 5. Sankey diagram of MSPA class transitions from 1990 to 2024 (areas in km^2).

Dynamics of ecological sources and corridors

Ecological sources contracted markedly over the past three decades (Fig. 6; Table 5). The source count rose from 23 in 1990 to 36 in 2010 and then fell sharply to 14 in 2024. The total source area declined monotonically from 9,190.8 $km^2$to 5,852.4 km^2. In 1990, one primary source of 6,061.0 km^2 dominated, accounting for 65.95% of the

source area. After 2000, the pattern became more polycentric. By 2024, the remaining primary source (2,781.5 km^2, 47.53%) again carried nearly half of the total, indicating consolidation into fewer patches, but the largest primary source shrank substantially. The mean source area increased only slightly from 399.6 to 418.0 km^2. Source grades were determined by natural divisions in CF_Central, with the annual thresholds detailed in Online Resources S7 and S9. In 1990, the attribute table identified 10 general, 12 secondary, and 1 primary source class. By 2024, the attribute table identified 9 general, 4 secondary, and 1 primary source class.

Table 5 Statistics of ecological sources by grade from 1990 to 2024. Source grades were assigned using natural breaks in CF_Central (Online Resources S7, S9).

Year	Grade	Count	Area (km^2)	Count share (%)	Area share (%)
1990	Primary	1	6 061.00	4.35	65.95
	Secondary	12	1 781.54	52.17	19.38
	General	10	1 348.26	43.48	14.67
	Total	23	9 190.79	100	100
2000	Primary	1	2 180.94	3.45	30.52
	Secondary	7	2 018.70	24.14	28.25
	General	21	2 945.19	72.41	41.22
	Total	29	7 144.83	100	100
2010	Primary	2	1 939.83	5.56	29.36
	Secondary	15	1 926.33	41.67	29.16
	General	19	2 740.98	52.78	41.49
	Total	36	6 607.13	100	100
2024	Primary	1	2 781.47	7.14	47.53
	Secondary	4	1 765.86	28.57	30.17
	General	9	1 305.08	64.29	22.30
	Total	14	5 852.41	100	100

Corridor systems fluctuated more strongly (Table 6; Fig. 7). The corridor count increased from 35 (755.9 km) in 1990 to a peak of 62 (1,307.3 km) in 2010, and then fell to 24 (800.5 km) in 2024. The grade structure also shifted. In 1990, primary and secondary corridors carried 31.73% and 50.69% of the total length, respectively. By 2010, tertiary corridors dominated with 86.48% of the total length. In 2024, the system rebalanced toward fewer but more functionally important links, with secondary corridors contributing 18.92% and tertiary corridors 73.36% of the total length (Wang et al. 2025). In 1990, this yielded 11 tertiary, 13 secondary, and 11 primary corridors. In 2024, this yielded 12 tertiary, 8 secondary, and 4 primary corridors. Corridor grades were assigned based on natural breaks in Current_Flow_Centrality; the annual thresholds are listed in Online Resources S7 and S9.

Table 6. Statistics of ecological corridors by grade from 1990 to 2024. Corridor grades were assigned based on natural breaks in the Current_Flow_Centrality (Online Resources S7 and S9).

Year	Grade	Count	Length (km)	Count share (%)	Length share (%)
1990	Primary	11	239.89	31.43	31.73
	Secondary	13	383.16	37.14	50.69
	Tertiary	11	132.89	31.43	17.58
	Total	35	755.90	100	100
2000	Primary	3	2.89	6.12	0.57

Year	Grade	Count	Length (km)	Count share (%)	Length share (%)
2010	Secondary	16	158.82	32.65	31.37
	Tertiary	30	344.64	61.22	68.06
	Total	49	506.35	100	100
	Primary	4	69.90	6.45	5.35
	Secondary	19	106.88	30.65	8.18
	Tertiary	39	1 130.51	62.90	86.48
	Total	62	1 307.29	100	100
2024	Primary	4	61.85	16.67	7.73
	Secondary	8	151.42	33.33	18.92
	Tertiary	12	587.19	50.00	73.36
	Total	24	800.45	100	100

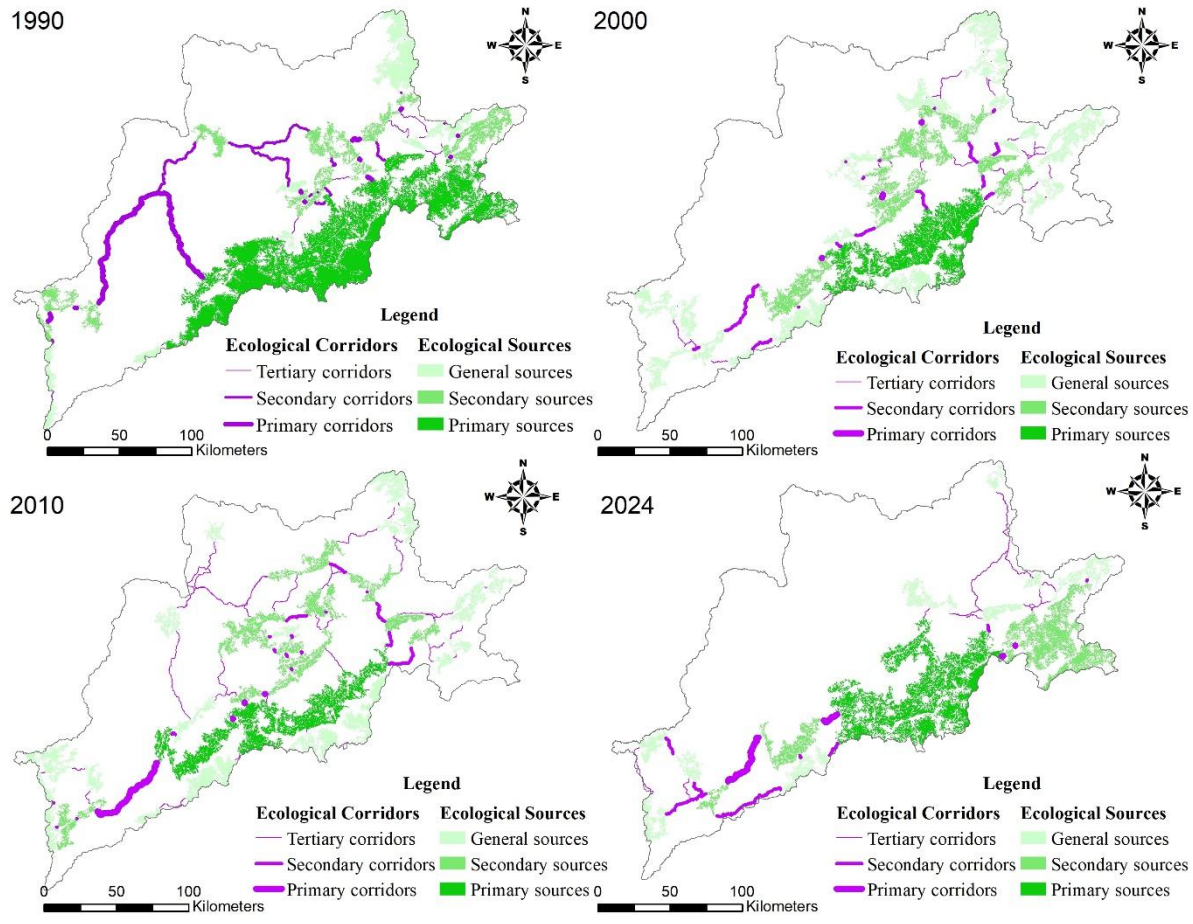


Fig. 6. Spatial distribution of ecological sources and ecological corridors in 1990, 2000, 2010 and 2024.

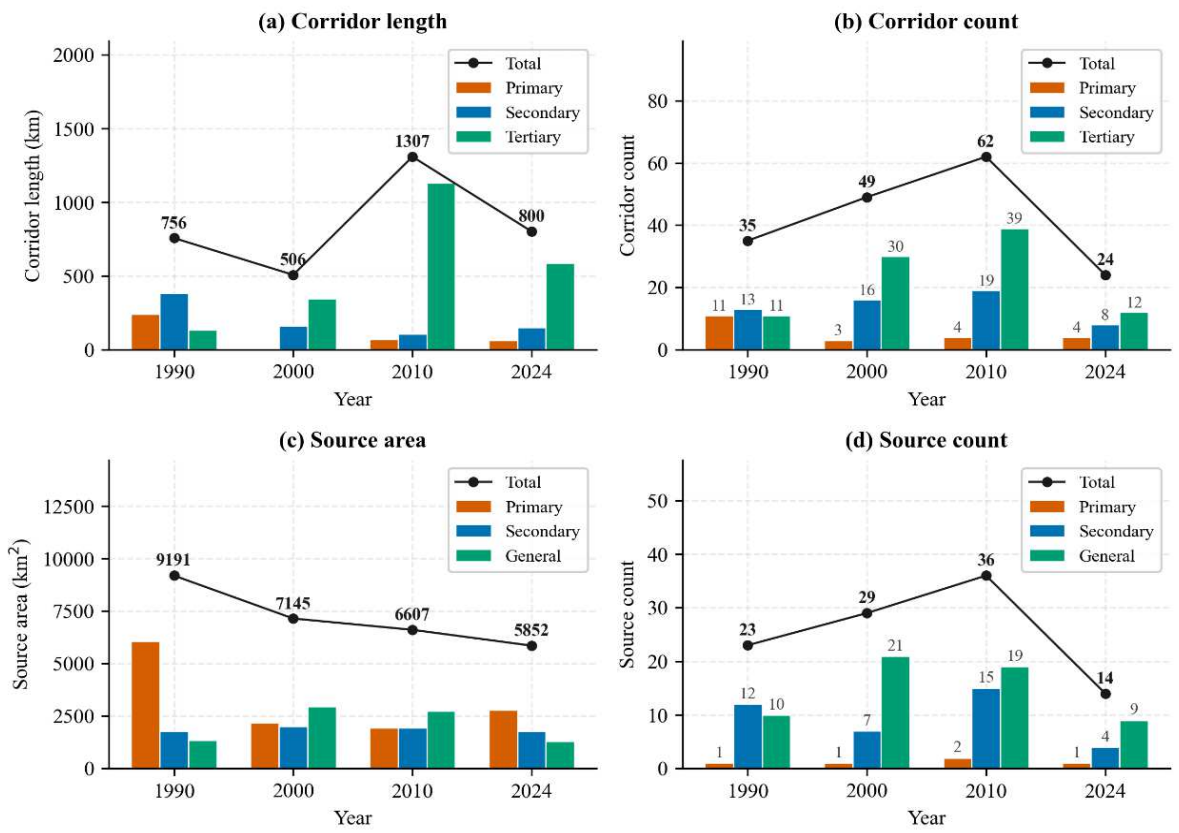


Fig. 7. Changes in ecological sources and corridors from 1990 to 2024: (a) corridor length, (b) corridor count, (c) source area, and (d) source count.

Resistance-surface sensitivity varied across the four periods (Fig. 8; Online Resource S11). All 16 year-scheme combinations retained a single connected source network; therefore, no baseline-connected source became fully disconnected. In 1990, the three alternatives reduced the primary corridor length share from 31.73% to 0.00-1.04%, and the reordered scheme removed all primary corridors and replaced 30 baseline source pairs. The 1990 current-layer Spearman correlations were 0.599, 0.529, and 0.323 for the compressed, expanded, and reordered schemes, respectively. In 2000 and 2010, the Spearman values remained above 0.92, and most primary corridor locations overlapped strongly, although the expanded scheme had 100-m cell Dice values of 0.391 and 0.634. In 2024, the three Spearman values were 0.956, 0.901, and 0.940; and the compressed scheme reduced the primary length share to 1.51% and had a primary corridor spatial Dice of 0.189. Therefore, the main topological conclusions remained stable, but corridor grades and primary corridor locations were conditional on the resistance assignment.

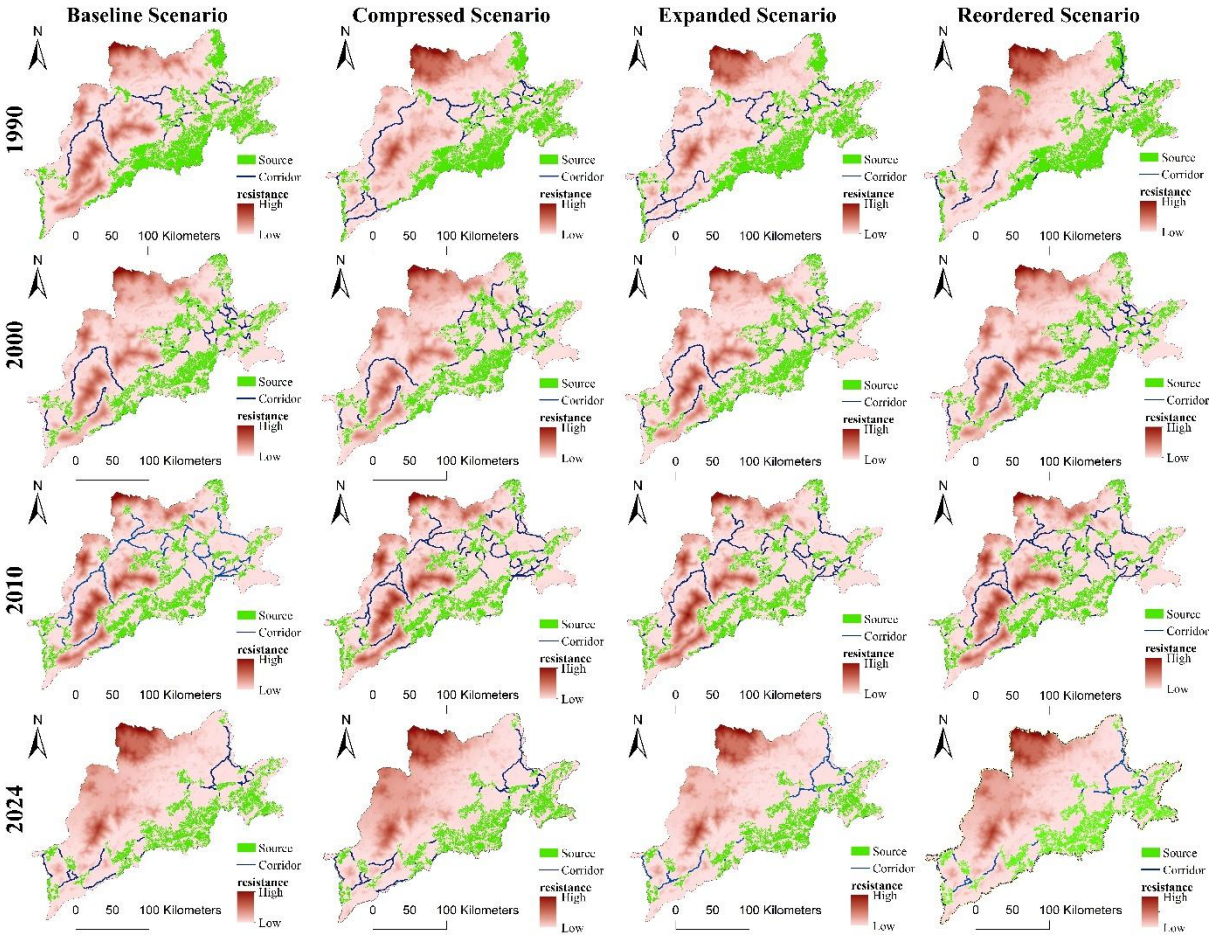


Fig. 8. Four-year resistance-surface sensitivity analysis. Rows show 1990, 2000, 2010, and 2024; columns show the baseline and compressed, expanded, and reordered resistance schemes.

Evolution of network topology

The four topological indices showed a consistent structural trend (Table 6). The circuitry index α increased from 0.317 in 1990 to 0.478 in 2024. This indicates a shift from a tree-like configuration toward a more circuitous structure with more redundant migration routes and greater topological redundancy (Zhang and Pan 2024). The connectivity index β remained above unity throughout (1.522 to 1.722) and rose overall, so each source patch was associated with more corridors. The slight decline in 2024 (1.714 versus 1.722 in 2010) was small. The cohesion index γ increased from 0.556 to 0.667, so the realized corridor network approached the theoretical maximum connectivity of a planar graph. Corridor density ρ fluctuated from 0.017 km/km² in 1990 to 0.012 km/km²in 2000. It peaked at 0.030 km/km² in 2010 and reached 0.018 km/km² in 2024, following annual variation in corridor length. The increases in α, β and γ coincided with a decline in source patches from 23 to 14. Here, α measures closed loops, β is the mean number of corridors per node, and γ is realized connectivity relative to the planar-graph maximum. The network therefore became structurally more compact and better connected: fewer source patches linked by a denser, more redundant corridor system (Cook 2002; Forman and Godron 1986).

Table 6. Topological indices of the ecological network for the four periods (V: number of sources; L: number of corridors; D: total corridor length; basin area A = 44,006.218 km²km^2).

Year	V	L	D (km)	α	β	γ	ρ (km/km²)
1990	23	35	755.904	0.317	1.522	0.556	0.017

Year	V	L	D (km)	α	β	γ	ρ (km/km²)
2000	29	49	506.349	0.396	1.690	0.605	0.012
2010	36	62	1 307.286	0.403	1.722	0.608	0.030
2024	14	24	800.450	0.478	1.714	0.667	0.018

4. Discussion

Why the intermediate trade-off scenario is preferred under the tested metric

The ESP selected under the tested metric fell between the two extreme decision rules. The maximum-type scenarios (S1 to S3) concentrate weight on the highest-ranked value at each pixel. They reward areas where a service is high but can ignore pixels with weak services. Their average efficiency remained the lowest in every period (1.0624, 1.0752, 1.0713, and 1.0838). The equal-weight scenario (S4) assumes that services are fully substitutable, an assumption commonly embedded when ESP studies average normalized layers; however, its efficiency remained below that of S5. The strongly minimum-type scenarios (S6 and S7) emphasize the lowest values of individual services. Across the four periods, their average conservation efficiency remained below that of S5, indicating that extreme weighting did not improve overall service protection. S5 ($\alpha = 2$) assigns greater weight to the lower-ranked values while retaining a small, nonzero weight for the highest values. It therefore favors pixels where several services are concurrently high without ignoring service deficits. Moderate aggregation rules approximate conservation preferences under ES trade-offs better than extreme rules (Bennett et al. 2009; Raudsepp-Hearne et al. 2010). Similar patterns appear in recent ESP applications (Guo et al. 2022; Yin et al. 2022; Yu et al. 2022). OWA makes these preferences explicit and testable in ESP research (Yager 1988, 1996). The selection of S5 is conditional on the priority-zone threshold and on the direction assigned to TN and TP export. S5 is therefore a basin-specific preference under the selected inputs, not a general rule.

Fragmentation of habitats versus consolidation of the network

The MSPA results and topology indices show the same overall trajectory. The core-area percentage share declined by 7.84 percentage points, while the core area declined by approximately 14.0% between 1990 and 2024, and the Sankey analysis shows that the dominant transition was the core → bridge. Large habitat blocks were gradually eroded into narrow connectors, a symptom of fragmentation driven by farmland expansion, settlement growth, and infrastructure in the intermountain basins (Vogt et al. 2007). At the same time, the circuitry, connectivity, and cohesion indices improved overall. The 2024 network is more looped and more densely interlinked than the 1990 network, although it contains only 14 sources. These trends can occur together: as peripheral and small patches were lost or merged, habitat with conservation value became concentrated in fewer sources, while the largest primary source shrank substantially. The corridor system connected these anchors with more redundant routes (Cook 2002; Jiang et al. 2024). The surge of tertiary corridors in 2010 (86.48% of corridor length) coincided with the period when ecological restoration programs were implemented in northern China (Ouyang et al. 2016). The timing is consistent with those programs, but the available land-cover series cannot establish causation. The later decline by 2024 suggests a consolidation phase in which weak links disappeared and the remaining backbone strengthened. Management may therefore consider prioritizing source and corridor classes that remain stable across resistance schemes, but these should be treated as conditional screening priorities rather than definitive planning zones until resistance values are validated.

Implications for ecological conservation in the basin

Three practical implications follow. First, the western and northern mountainous core areas, which include the persistent primary sources, could be treated as candidate strict protection zones because these areas jointly support carbon storage, soil retention and habitat quality. Second, the river-valley belt toward the Guanting Reservoir, where water-yield and nutrient export-control efficiencies are highest, could be considered as a buffer zone with riparian vegetation restoration. Such zoning would require socioeconomic feasibility checks. Third, the bridge-class areas, whose share has grown to 40.86%, could be treated as cost-effective candidate targets for corridor consolidation. Small investments in stepping-stone restoration along existing bridges can maintain the rising α, β and γ values at relatively low cost (Wang et al. 2025). These zoning options are model-based screening priorities and would require resistance validation, local socioeconomic feasibility checks and field verification before implementation.

Limitations and outlook

Several limitations should be acknowledged. First, ES quantification relies on InVEST with literature-based parameters. Therefore, the service outputs should be interpreted as model-based screening maps, and no independent field validation was available for water yield, nutrient export or carbon pools. Because A3 is a static LULC-mapped carbon-density result, its sensitivity mainly reflects uncertainty in the LULC classification and carbon-pool values rather than independent biophysical measurements. Second, the MSPA-class resistance assignment is transparent and reproducible, but it fixes resistance at the class level. Four-year sensitivity tests with three alternative resistance surfaces retained the overall connected network, but corridor grades and primary corridor locations changed materially, especially in 1990. Temporal comparisons therefore remain conditional on this class-based resistance assignment. Current-flow corridors could also be cross-validated against least-cost-path alternatives (Adriaensen et al. 2003). Third, the planar-graph abstraction ignores corridor width, quality, directionality and patch stability. Future work could weight edges by resistance or flow and integrate patch stability with network connectivity (Jiang et al. 2024). Dynamic connectivity could be tested under land-use and future-scenario simulations (Forman and Godron 1986; Cook 2002; Li et al. 2023; Wu et al. 2025). Fourth, the four-period sampling may mask finer fluctuations. Annual land-cover products now available (Yang and Huang 2026) would allow yearly-resolution application. Changes could then be attributed more precisely to specific policy programs. The selected S5 is therefore interpreted as a basin-specific preference, not a general rule. Sensitivity analysis also showed that S5 is spatially less close to the equal-weight baseline than α = 0.1 to 1, and that the priority area is most sensitive to service A3.

5. Conclusions

This study constructed and analyzed the ecological security pattern of the upper Yongding River Basin by coupling OWA-based multi-scenario trade-off analysis with MSPA-based source extraction and Circuitscape-based corridor identification. Six ESs were quantified for 1990, 2000, 2010 and 2024. Seven OWA scenarios spanning weighting parameters from 0.001 to 1000 were compared by conservation efficiency, and the moderate weighting scenario (S5, α = 2) was the preferred scenario under the tested metric in all four periods. Under this scenario, the ESP changed in two ways. The MSPA core share declined from 56.10% to 48.26%, while the bridge share rose to 40.86%. Ecological sources fell from 23 patches (9,190.8 km^2) in 1990 to 14 patches (5,852.4 km^2) in 2024. At

the same time, the circuitry, connectivity and cohesion indices rose overall to 0.478, 1.714 and 0.667. The network shifted toward fewer source patches, while the largest primary source shrank substantially; the remaining sources were interconnected by a denser, more redundant corridor system. As a technical screening framework, the workflow applies ES trade-offs to conservation planning and supports candidate identification for source protection, corridor consolidation and restoration zoning in the basin; these priorities remain conditional on resistance and validation. It may be applied to other basins only after independent validation, and the selected scenario is not presented as a general preference.

Supplementary Materials

The following supplementary files are provided as Online Resources and are submitted separately from the main manuscript.

Table S1. Annual water yield biophysical table (S1_AWY_biophysical_table.csv).

Table S2. Carbon storage and sequestration carbon pools (S2_Carbon_ pools. csv).

Table S3. Habitat quality land-use sensitivity table (S3_HQ_sensitivity.csv).

Table S4. Habitat quality threat table (S4_HQ_threats.csv).

Table S5. Nutrient delivery ratio biophysical table (S5_NDR_biophysical_table.csv).

Table S6. Sediment delivery ratio USLE factors (S6_SDR_USLE_factors.csv).

Table S7. Linkage Mapper natural-break classification summary (S7_LinkageMapper_Natural_Breaks_clean.csv; Supplementary_Table_S7_LinkageMapper_Natural_Breaks.docx; S7_LinkageMapper_Natural_Breaks.pdf).

Table S8. OWA conservation efficiency by scenario and period (S8_OWA_Conservation_Efficiency_1990_2024.csv; S8_OWA_Conservation_Efficiency_1990_2024.docx; S8_OWA_Conservation_Efficiency_1990_2024.pdf).

Table S9. ArcMap natural-break reclassification statistics for corridor length share and source area (S9_LinkageMapper_Reclassification_Statistics.csv; S9_LinkageMapper_Reclassification_Statistics.docx).

Table S10. Summary of OWA sensitivity analyses (S10_OWA_Sensitivity_Summary.csv; S10_OWA_Sensitivity_Summary.docx).

Table S11. Resistance-surface sensitivity summary (S11_Resistance_Sensitivity_Summary.docx; S11_Resistance_Sensitivity_Summary.pdf; centrality_rank_sensitivity_all_years.csv; corridor_and_connectivity_sensitivity_all_years.csv; current_layer_sensitivity_metrics_all_years.csv; primary_corridor_spatial_overlap_all_years.csv).

References

Adriaensen F Chardon JP De Blust G Swinnen E Villalba S Gulinck H Matthysen E (2003) The application of 'least-cost' modelling as a functional landscape model. Landscape and Urban Planning 64:233–247. https://doi.org/10.1016/s0169-2046(02)00242-6

Bennett EM Peterson GD Gordon LJ (2009) Understanding relationships among multiple ecosystem services. Ecology Letters 12:1394–1404. https://doi.org/10.1111/j.1461-0248.2009.01387.x

Braat LC, de Groot R (2012) The ecosystem services agenda: bridging the worlds of natural science and economics, conservation and development, and public and private policy. Ecosystem Services 1:4–15. https://doi.org/10.1016/j.ecoser.2012.07.007

Burkhard B Kroll F Nedkov S Müller F (2012) Mapping ecosystem service supply, demand and budgets. Ecological Indicators 21:17–29. https://doi.org/10.1016/j.ecolind.2011.06.019

Cook EA (2002) Landscape structure indices for assessing urban ecological networks. Landscape and Urban Planning 58:269–280. https://doi.org/10.1016/s0169-2046(01)00226-2

Costanza R, d'Arge R, de Groot R Farber S Grasso M Hannon B Limburg K Naeem S O'Neill RV Paruelo J Raskin RG Sutton P, van den Belt M (1997) The value of the world's ecosystem services and natural capital. Nature 387:253–260. https://doi.org/10.1038/387253a0

Crossman ND Burkhard B Nedkov S Willemen L Petz K Palomo I Drakou EG Martín-López B McPhearson T Boyanova K Alkemade R Egoh B Dunbar MB Maes J (2013) A blueprint for mapping and modelling ecosystem services. Ecosystem Services 4:4–14. https://doi.org/10.1016/j.ecoser.2013.02.001

Daily GC (1997) Nature's Services: Societal Dependence on Natural Ecosystems. Island Press, Washington, DC

Donohue RJ Roderick ML McVicar TR (2012) Roots, storms and soil pores: incorporating key ecohydrological processes into Budyko's hydrological model. Journal of Hydrology 436–437:35–50. https://doi.org/10.1016/j.jhydrol.2012.02.028

Forman RTT Godron M (1986) Landscape Ecology. John Wiley & Sons, New York

Guo M Cong X Zheng H Zhang MJ Wang LJ Gong JW Ma S (2022) Integrating the ordered weighted averaging method to establish an ecological security pattern for the Jianghuai Ecological Economic Zone in China: Synergistic intraregional development. Ecological Indicators 135:108543. https://doi.org/10.1016/j.ecolind.2022.108543

Haggett P Chorley RJ (1969) Network Analysis in Geography. Edward Arnold, London

Jiang H Peng J Liu M Dong J Ma C (2024) Integrating patch stability and network connectivity to optimize ecological security pattern. Landscape Ecology 39:54. https://doi.org/10.1007/s10980-024-01852-w

Kansky KJ (1963) Structure of Transportation Networks: Relationships between Network Geometry and Regional Characteristics. Research Paper No. 84, Department of Geography, University of Chicago, Chicago

Li F Zhao Y Zhao Y (2024) Construction and optimization of ecological network based on morphological spatial pattern analysis and minimum cumulative resistance models in Haihe River Basin. Ecohydrology 17:e2620. https://doi.org/10.1002/eco.2620

Li L Huang X Wu D Yang H (2023) Construction of ecological security pattern adapting to future land use change in Pearl River Delta, China. Applied Geography 154:102946. https://doi.org/10.1016/j.apgeog.2023.102946

Liu X Su Y Li Z Zhang S (2023) Constructing ecological security patterns based on ecosystem services trade-offs and ecological sensitivity: A case study of Shenzhen metropolitan area, China. Ecological Indicators 154:110626. https://doi.org/10.1016/j.ecolind.2023.110626

McRae BH Dickson BG Keitt TH Shah VB (2008) Using circuit theory to model connectivity in ecology, evolution, and conservation. Ecology 89:2712–2724. https://doi.org/10.1890/07-1861.1

Millennium Ecosystem Assessment (2005) Ecosystems and Human Well-being: Synthesis. Island Press, Washington, DC

Ouyang Z Zheng H Xiao Y Polasky S Liu J Xu W Wang Q Zhang L Xiao Y Rao E Jiang L Lu F Wang X Yang G Gong S Wu B Zeng Y Yang W Daily GC (2016) Improvements in ecosystem services from investments in natural capital. Science 352:1455–1459. https://doi.org/10.1126/science.aaf2295

Pan J Li L (2021) Optimization of ecological security pattern in Gansu section of the Yellow River Basin using OWA and circuit model. Transactions of the Chinese Society of Agricultural Engineering 37(3):259-268. https://doi.org/10.11975/j.issn.1002-6819.2021.03.031

Peng J Pan Y Liu Y Zhao H Wang Y (2018) Linking ecological degradation risk to identify ecological security patterns in a rapidly urbanizing landscape. Habitat International 71:110–124. https://doi.org/10.1016/j.habitatint.2017.11.010

Raudsepp-Hearne C Peterson GD Bennett EM (2010) Ecosystem service bundles for analyzing tradeoffs in diverse landscapes. Proceedings of the National Academy of Sciences 107:5242–5247. https://doi.org/10.1073/pnas.0907284107

Seppelt R Dormann CF Eppink FV Lautenbach S Schmidt S (2011) A quantitative review of ecosystem service studies: approaches, shortcomings and the road ahead. Journal of Applied Ecology 48:630–636. https://doi.org/10.1111/j.1365-2664.2010.01952.x

Sharp R Douglass J Wolny S Arkema K Bernhardt J Bierbower W Chaumont N Denu D Fisher D Frazier K, et al. (2020) InVEST 3.19.0 User's Guide. The Natural Capital Project, Stanford University, University of Minnesota, The Nature Conservancy, and World Wildlife Fund

Soille P Vogt P (2009) Morphological segmentation of binary patterns. Pattern Recognition Letters 30:456–459. https://doi.org/10.1016/j.patrec.2008.10.015

Vogt P Riitters KH Estreguil C Kozak J Wade TG Wickham JD (2007) Mapping spatial patterns with morphological image processing. Landscape Ecology 22(2):171–177. https://doi.org/10.1007/s10980-006-9013-2

Wang S Zhang R Wang J Li Q Wang R Li Y Zhang L (2025) Identification and optimization of ecological corridors in the middle reaches of the Yellow River Basin. Journal of Cleaner Production 512:145676. https://doi.org/10.1016/j.jclepro.2025.145676

Wischmeier WH Smith DD (1978) Predicting Rainfall Erosion Losses: A Guide to Conservation Planning. USDA Agriculture Handbook No. 537, Washington, DC

Wu J (2013) Landscape sustainability science: ecosystem services and human well-being in changing landscapes. Landscape Ecology 28(6):999–1023. https://doi.org/10.1007/s10980-013-9890-0

Wu Q Cao Y Zhang Y Su D Fang X (2025) Linking ecosystem services trade-offs, human preferences and future scenario simulations to ecological security patterns: a novel methodology for reconciling conflicting ecological functions. Applied Geography 176:103534. https://doi.org/10.1016/j.apgeog.2025.103534

Yager RR (1988) On ordered weighted averaging aggregation operators in multicriteria decisionmaking. IEEE Transactions on Systems, Man, and Cybernetics 18:183–190. https://doi.org/10.1109/21.87068

Yager RR (1996) Quantifier guided aggregation using OWA operators. International Journal of Intelligent Systems 119(1):49–73. https://doi.org/10.1002/(sici)1098-111x(199601)11:1<49::aid-int3>3.0.co;2-z

Yang J Huang X (2026) The 30 m annual land cover datasets and its dynamics in China from 1985 to 2025. Earth System Science Data 13:3907-3925. https://doi.org/10.5281/zenodo.18180184

Yin L Dai E Guan M Zhang B (2022) A novel approach for the identification of conservation priority areas in mountainous regions based on balancing multiple ecosystem services: a case study in the Hengduan Mountain region. Global Ecology and Conservation 38:e02195. https://doi.org/10.1016/j.gecco.2022.e02195

Yu K (1996) Security patterns and surface model in landscape ecological planning. Landscape and Urban Planning 36:1–17. https://doi.org/10.1016/s0169-2046(96)00331-3

Yu H Gu X Liu G Fan X Zhao Q Zhang Q (2022) Construction of regional ecological security patterns based on multi-criteria decision making and circuit theory. Remote Sensing 14:527. https://doi.org/10.3390/rs14030527

Zhai T Huang L (2022) Linking MSPA and circuit theory to identify the spatial range of ecological networks and its priority areas for conservation and restoration in urban agglomeration. Frontiers in Ecology and Evolution 10:828979. https://doi.org/10.3389/fevo.2022.828979

Zhang K Pan J (2024) Evaluation of ecological network resilience using OWA and attack scenario simulation in the Gansu section of the Yellow River Basin, NW China. Environmental Research Communications 6:085016. https://doi.org/10.1088/2515-7620/ad6d3d

Zhang F Liu X Jia Y (2025) Construction and evolution of river basin ecological network based on circuit theory and MSPA: A case study of Dawen River Basin. Ecological Modelling 510:111364. https://doi.org/10.1016/j.ecolmodel.2025.111364

Zhang L Fu B Lü Y Zeng Y (2015) Balancing multiple ecosystem services in conservation priority setting. Landscape Ecology 30(3):535-546. https://doi.org/10.1007/s10980-014-0106-z

Statements and Declarations

Funding

This work was supported by the National Science and Technology Major Project of China (grant number 2025ZD1202102) and the Key Research and Development Program of Hebei Province (grant number 22376201D).

Competing Interests

The authors have no relevant financial or non-financial interests to disclose.

Author Contributions

Yan Jiang: conceptualization, methodology, supervision, writing - original draft. Gang Wang: data curation, formal analysis, writing - review & editing. Xiaoyan Zhang: resources, funding acquisition, writing - review & editing. Jingfeng Hu: software, validation, investigation, writing - review & editing.

Data Availability

The data supporting the findings of this study are available from the corresponding author, Yan Jiang (jiangyan@iwhr.com), on reasonable request. Analysis code, InVEST parameter tables, Linkage Mapper and Circuitscape configurations, and derived outputs are described in the Supplementary Materials and can also be obtained from the corresponding author.

Supplementary Files

This is a list of supplementary files associated with this preprint. Click to download.

- SupplementaryTable.docx